Narrow-Band-Gap Conjugated Chromophores with Extended Molecular Lengths

Xiaofeng Liu,[†,‡] Yanming Sun,[†,§] Louis A. Perez,[†,∇] Wen Wen,[†,‡] Michael F. Toney,[#] Alan J. Heeger,[†,§] and Guillermo C. Bazan*,[†,‡,∇]

[†]Center for Polymers and Organic Solids, [‡]Department of Chemistry and Biochemistry, [§]Department of Physics, and [∇]Department of Materials, University of California, Santa Barbara, California 93106, United States
[#]Stanford Synchrotron Radiation Lightsource, SLAC National Accelerator Laboratory, Menlo Park, California 94025, United States

Ⓢ *Supporting Information*

ABSTRACT: The influence of extending the molecular length of donor−acceptor chromophores on properties relevant to organic optoelectronic devices has been studied by using two new narrow-band-gap systems. Most significantly, we find that the higher molecular weight systems exhibit higher thermal stabilities (beyond 200 °C) when introduced into field effect transistor devices. It is also possible to fabricate bulk heterojunction solar cells using $PC_{61}BM$ with power conversion efficiencies >6%. These high values are not heavily influenced by the blend composition and are achieved without the influence of solvent additives or postdeposition thermal annealing.

There is emerging interest in the use of chromophores with discrete molecular dimensions as replacements for narrow-band-gap conjugated polymers in solution-processed bulk heterojunction (BHJ) organic photovoltaic (OPV) devices.[1] Both classes of materials are designed similarly in terms of orbital energy levels, which affect the open-circuit voltage (V_{oc}) of the cells, and absorption profiles, which provide efficient overlap with solar light.[2] Molecular design and processing conditions are also important for achieving homogeneous thin films that yield appropriate BHJ morphologies and do not interact adversely with the electrodes.[3] Evidence accumulated thus far points to polymers and molecules requiring somewhat different thin-film processing conditions to achieve the most efficient device performances.[4] The general structural characteristics of molecular BHJ solar cells are also considerably less well detailed compared to their polymeric counterparts.[5]

Several arguments have been put forward in favor of the molecular materials approach[6] relative to conjugated polymers.[7] These include reduced batch-to-batch variability, absence of a molecular weight distribution, ease of purification, and greater solubility in common solvents. Polymeric systems, however, benefit from a vast literature on optimal film casting conditions, postdeposition modifications, and device architectures that lead to high power conversion efficiencies (PCEs).[8] Polymer thin films are also easier to process and are more resistant to dewetting.[9] An important additional consideration is the possibility that polymers may provide more stable phases and therefore longer device lifetimes, although no systematic study or guidelines that have emerged within this context.

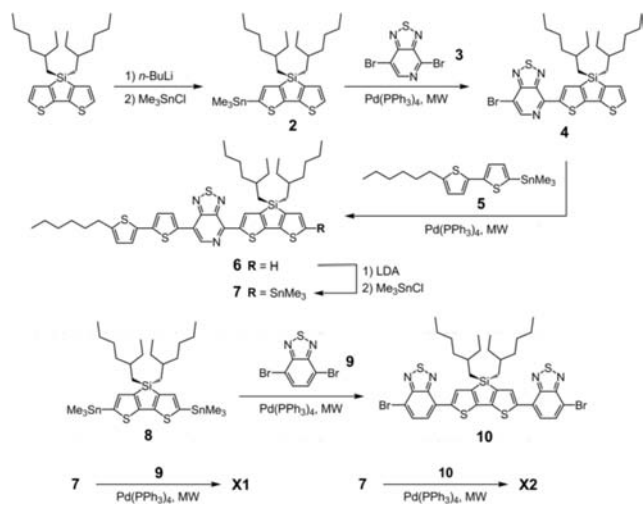## Scheme 1. Chemical Structures of Narrow-Band-Gap Molecules
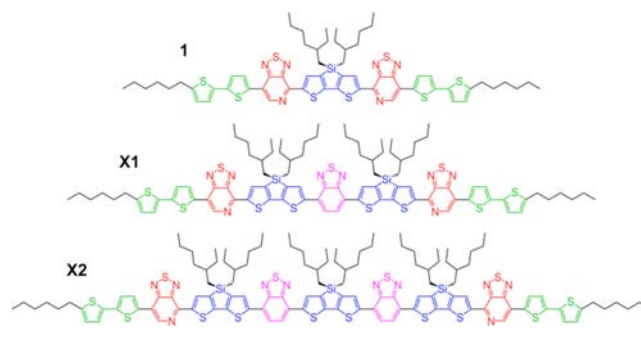
Recent reports have described the use of molecules with a variety of structural frameworks that provide PCE values in the 6−7% range.[10] One specific class is based on the D^1-A-D^2-A-D^1 framework, for example **1** in Scheme 1,[6b] where D^1 and D^2 represent different donor units denoted as green and blue fragments, respectively. In this work we use two model compounds to explore the influence of chromophore elongation. The two new molecules used for this purpose, which can be expressed as D^1-A^1-D^2-A^2-D^2-A^1-D^1 (**X1**; A^1, red; A^2, purple) and D^1-A^1-D^2-A^2-D^2-A^2-D^2-A^1-D^1 (**X2**), are also shown in Scheme 1. Since the electron-rich (D) and -poor (A) moieties are similar to the structural units in D-A polymeric analogues, these oligomeric molecules provide a unique bridge to study how relevant properties change as one transitions from molecules to polymers.

Compounds **X1** and **X2** were synthesized via a microwave-assisted Stille coupling reaction[7b] between the monostannylated molecular "wing" of 5-{(4-(7-hexylthiophen-2-yl)thiophen-2-yl)[1,2,5]thiadiazolo[3,4-*c*]pyridine)}-3,3′-bis(2-ethylhexyl)-silylene-2,2′-bithiophene) (**7**) and molecular "cores" of either 4,7-dibromobenzo[2,1,3]thiadiazole (**9**) or 5,5′-bis[4-(7-bromobenzo[2,1,3]thiadiazole)]-3,3′-bis(2-ethylhexyl)silylene-2,2′-bithiophene (**10**), as shown in Scheme 2. Synthesis and characterization are described in the Supporting Information (SI). The chemical structures of **X1** and **X2** were confirmed by NMR spectroscopy and mass spectrometry. The ^{1}H NMR spectrum of **X1** shows well-defined resonance peaks, while **X2**

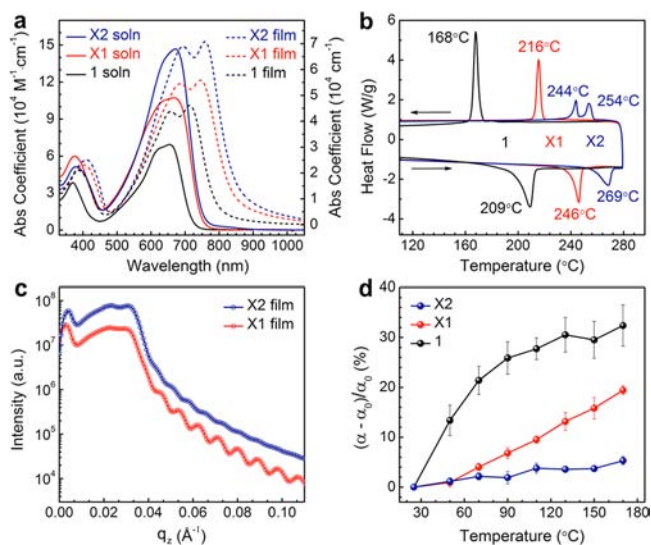**Scheme 2. Synthetic Entry into X1 and X2**

Figure 1. (a) UV/vis absorption spectra of **1**, **X1**, and **X2** in solution and in the solid state. (b) Phase transitions measured by DSC showing melting (T_m) and crystallization (T_c) temperatures. (c) Thin-film XRR curves; fringe spacing was used to obtain the film thickness. (d) Temperature dependence of extinction coefficients in the solid state.

gives broadened, featureless signals (SI). This is most reasonably due to the higher molecular weight of **X2** (2287.7 g/mol) compared to **X1** (1736.8 g/mol). Because of the larger number of ethylhexyl side groups, **X1** and **X2** are more soluble in CHCl$_3$ (>50 mg/mL) than **1** (25 mg/mL) at 25 °C.[6b]

Figure 1a shows the absorption properties in CHCl$_3$ and in the solid state. Similar to **1**, **X1** and **X2** exhibit bands centered at 670 and 672 nm in CHCl$_3$ solutions, with molar absorption coefficients of 1.07×10^5 and 1.47×10^5 M^{-1} cm^{-1}, respectively. The absorption spectra of thin films of **1**, **X1**, and **X2**, obtained via spin-casting CHCl$_3$ solutions (1%, w/v) atop glass exhibit a red shift in absorption onset of 100, 104, and 115 nm, respectively. Compared to the film absorption coefficient (α) of 4.61×10^4 cm^{-1} for **1**, α was determined as 5.59×10^4 (**X1**) and 7.08×10^4 cm^{-1} (**X2**); these values are typical for polymers that contain thiadiazolo[3,4-c]pyridine.[11] Optical band-gaps were determined from absorption onsets of **1**, **X1**, and **X2** as 1.52, 1.44, and 1.41 eV, respectively. The continuous decrease of band-gap reflects the increased electron delocalization.

Measurements by cyclic voltammetry (CV) provide band-gaps of 1.59 (**1**), 1.44 (**X1**), and 1.33 eV (**X2**), which are close to those estimated from optical measurements. Thus, adding an extra D-A segment to **1** (i.e., **X1**) does not bring an obvious change in oxidation potential, with two oxidation processes and a HOMO energy level of −5.17 eV (for **1**: −5.19 eV). Interestingly, the larger molecular size of **X2** results in four reversible oxidation peaks under the same bias; i.e., four electrons can be donated per molecule. The HOMO level of **X2** also increased to −5.04 eV. It is worth pointing out that multi-charged species were observed in field desorption (FD) mass spectroscopy, in which M$^+$ and M^{2+} were visible for **1**; M$^+$, M^{2+}, and M^{3+} were observed for **X1**, while an additional M^{4+} was shown for **X2** (SI). In a typical FD experiment, molecules are ionized by a high-potential electric field. Therefore, the emergence of triple and quadruple charged species in **X1** and **X2** under identical conditions indicates an increased ability to support multiple oxidized states. This observation is consistent with the multi-oxidation process obtained from CV.

Figure 1b shows the thermal transitions as determined by differential scanning calorimetry (DSC). Melting temperatures (T_m) of 246 and 269 °C were observed for **X1** and **X2**, 37 and 60 °C higher than for **1** (209 °C), respectively. Interestingly,

X2 exhibits two exothermic peaks at 254 and 244 °C upon cooling, which may be attributed to monotropic liquid crystalline behavior.[12] Our current thinking is that the additional segments in **X2** increase molecular flexibility, which may account for the semi-stable mesophase during the cooling process. Despite these uncertainties, it is worth pointing out that extending the length of the molecular framework leads to a considerably more stable crystalline phase.

Thin-film absorption spectra as a function of thermal annealing temperature were collected to obtain additional information on thermal transitions. Profilometry revealed that the thicknesses of all films were on the order of 70 ± 5 nm. X-ray reflectivity (XRR) measurements (Figure 1c) were also used to calculate film thickness (SI),[13] giving 69 ± 1 and 73 ± 1 nm for **X1** and **X2**, respectively, in agreement with profilometry. The absorption spectra were recorded at room temperature and after annealing at various temperatures (SI). Note that the thermal treatment has a negligible effect on film thickness. Figure 1d shows a plot of film absorption coefficient changes $(\alpha - \alpha_0)/\alpha_0$ versus annealing temperature up to 170 °C for all three materials, where α is film absorption coefficient after annealing at different temperatures, and α_0 is that measured at room temperature. The value of α was recorded at λ_{max} for each material, 725 (**1**), 748 (**X1**), and 758 nm (**X2**). Compound **1** shows the most sensitive temperature dependence of α, with an increase of ~30% over α_0 beyond 120 °C. **X1** exhibited low temperature sensitivity below 60 °C, with a moderate increase as the annealing temperature was further increased, reaching a value of ~20% higher than α_0 at 170 °C. Surprisingly, very small changes were observed with **X2**, with an increase in α of less than 5%. Therefore, the optical properties of the longer chromophores are less sensitive to thermal effects.

The influence of thermal annealing on the molecular orientation in **X1** and **X2** thin films was investigated using grazing incidence wide-angle X-ray scattering (GIWAXS) (Figure 2). All the films were spin-casted from 1% CHCl$_3$ solutions atop a silicon wafer at 1500 rpm. From Figure 2, both as-cast films of **X1** and **X2** exhibit strong reflections along all
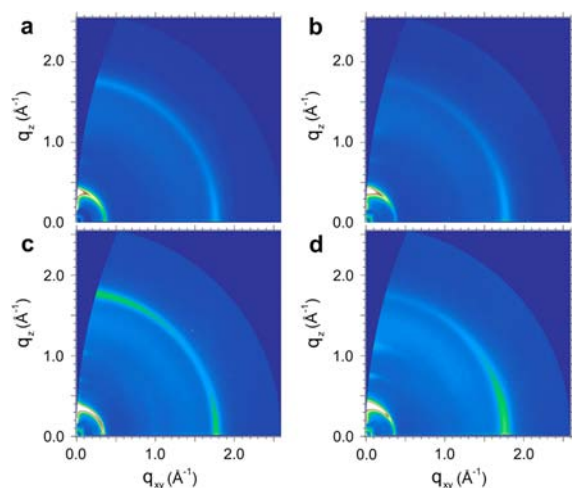
Figure 2. GIWAXS profiles of as-cast films of **X1** (a) and **X2** (b) spin-coated from 1% CHCl$_3$ solution and the films of **X1** (c) and **X2** (d) after thermal annealing at 100 °C for 2 min.

polar angles at q values of 0.38 and 0.39 Å^{-1}, respectively, which correspond to the alkyl spacing direction. From the integrated line profiles (SI), the "lamellar" spacing can be determined as 16.5 and 16.1 Å for **X1** and **X2**, respectively. The $\pi-\pi$ stacking peak, at $q = 1.78$ Å^{-1}, is equally distributed along all polar angles for **X1**, showing that the $\pi-\pi$ stacking direction in the crystallites of **X1** is randomly oriented within the as-cast film. In comparison, **X2** shows a more pronounced peak along the in-plane direction (Figure 2b), which indicates a greater preference for edge-on molecular orientation relative to the silicon surface. Both films give a $\pi-\pi$ stacking spacing of 3.5 Å. Thermal annealing (100 °C for 2 min) of **X1** films leads to a more intense $\pi-\pi$ stacking reflection near both the in-plane and out-of-plane directions, as well as a slight decrease in d spacing (SI), indicating an additional molecular organization upon thermal treatment. For **X2**, further thermal treatment brought only a minimal change of the molecular orientation, except for a relative increase of intensity. These observations suggest that the **X2** thin film is able to retain the same molecular orientation upon treatment at higher temperature, which agrees with the minor change in film absorption coefficient in Figure 1d.

Organic field effect transistors (OFETs) were used to measure charge carrier mobilities (Figure 3a). The as-cast films under identical preparation condition for **1**, **X1**, and **X2** give hole mobilities of 0.02, 0.01, and 0.006 cm^2/V·s, respectively (SI). Compound **1** showed the highest mobility

after thermal annealing at 80 °C (0.03 cm^2/V·s), followed by a sharp drop upon further annealing; the device ultimately failed when heated beyond 150 °C. In contrast, the highest mobilities of **X1** and **X2** appeared after annealing at 100 °C (0.018 cm^2/V·s) and 120 °C (0.01 cm^2/V·s). Devices with **X1** and **X2** show thermal stability beyond 200 °C, with moderate mobility of **X1** at 230 °C (0.003 cm^2/V·s) and **X2** at 250 °C (0.0026 cm^2/V·s). It is evident from this set of experiments that extension of molecular characteristics yields gains in thermal stability while maintaining useful charge carrier mobilities and therefore provides an important consideration for designing new materials that can endure wider environmental variability.

As a final set of evaluations, the photovoltaic properties of **X1** and **X2** were investigated with a device structure of indium tin oxide (ITO)/MoO$_x$/**X1** or **X2**:[6,6]-phenyl-C61-butyric acid methyl ester (PC$_{61}$BM)/Al.[14] Active layers were spin-coated from CHCl$_3$ solution, with a total solid concentration of 2% (w/v). Photovoltaic parameters obtained under AM 1.5G at 100 mA/cm^2 are summarized in Table 1. An optimal weight

Table 1. Photovoltaic Characteristics of Molecule Solar Cells

molecule:PC$_{61}$BM (wt:wt)		J_{sc} (mA/cm^2)	V_{oc} (V)	FF (%)	PCE (%)
X1[a]	70:30	12.3	0.70	56	4.8
	60:40	13.6	0.71	60	5.8
	50:50	13.8	0.72	53	5.2
X2[b]	60:40	14.6	0.68	64	6.4
	50:50	15.2	0.66	65	6.5
	40:60	15.2	0.65	61	6.0

[a]Annealed at 100 °C for 10 min before cathode deposition. [b]Devices fabricated without thermal treatment.

ratio of 60:40 was observed with **X1**, giving a device with PCE = 5.8%, upon thermal annealing at 100 °C for 10 min, with a short-circuit current (J_{sc}) of 13.6 mA/cm^2, V_{oc} of 0.71 V, and fill factor (FF) of 60% (Figure 3b). For **X2**, however, highest efficiency (J_{sc} = 15.2 mA/cm^2, V_{oc} = 0.66 V, FF = 65%, PCE = 6.5%) was obtained with a weight ratio of 50:50. Thermal annealing of **X2**/PC$_{61}$BM has no effect on the device efficiency, consistent with the GIWAXS data that show no changes on annealing. These PCEs are among the highest values reported to date for PC$_{61}$BM-based molecular solution-processable solar cells.[10c,15]

Some comments on the differences in device performance follow. It is worth noting that for **1**, in the absence of solvent additives or thermal annealing, one obtains the best performance (PCE = 4.5%) at a **1**:PC$_{71}$BM composition ratio of 70:30.[10a] These loadings of molecule donor relative to fullerene greater than 50% are often observed with discrete molecular systems vs conjugated polymer counterparts.[10,16] The data in Table 1 reveal that increases in the molecular length (and weight) of the systems studied here lead to a modification in the optimal device composition ratio: 60:40 for **X1**:PC$_{61}$BM and 50:50 for **X2**:PC$_{61}$BM, similar to those broadly required for conjugated polymers.[17] Of further note is that the optimal performance achieved for the **X2**:PC$_{61}$BM combination is relatively insensitive to the composition ratio (SI).

In conclusion, two new molecules, namely **X1** and **X2**, were designed and synthesized with the goal of obtaining insight into the role of molecular size on relevant properties that influence function in optoelectronic devices. Both **X1** and **X2** contain electron-rich and electron-poor heterocyclic subunits that lead
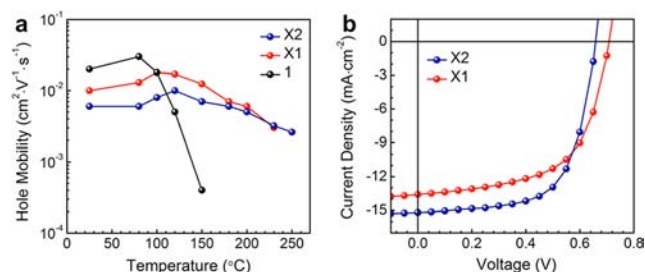

Figure 3. (a) Hole mobility as a function of annealing temperature for **1**, **X1**, and **X2**. (b) J–V curves of the BHJ solar cell devices with the highest performance obtained by blending PC$_{61}$BM with **X1** and **X2**, respectively.

to appropriate optical profiles and orbital energy levels to function as the donor component in BHJ solar cell devices. With increases in molecular size one observes a systematic increase in melting transitions and the optical features of thin films. Concomitantly, one finds more thermally stable optical absorption features and hole mobilities within OFET configurations. The performances of **X1**:PC$_{61}$BM and **X2**:PC$_{61}$BM are also close to the best reported in the literature for molecular BHJ solar cells. Perhaps more importantly, one finds that interesting BHJ composition trends emerge. Specifically, the optimal BHJ ratio approximates those of conjugated polymer cells, and the **X2**:PC$_{61}$BM blend performance is quite consistent despite variations in blend composition. These studies suggest that there is value in increasing molecular size within structurally well-defined organic semiconductors. Whether these advantages outweigh the additional upfront investment in synthesis is a topic of future work.

■ ASSOCIATED CONTENT

Ⓢ Supporting Information

Synthesis and characterization of **X1** and **X2**; detailed preparation procedure for OFETs and solar cells; *J−V* curves and EQE spectra at different D/A ratios. This material is available free of charge via the Internet at http://pubs.acs.org.

■ AUTHOR INFORMATION

Corresponding Author
bazan@chem.ucsb.edu

Notes
The authors declare no competing financial interest.

■ ACKNOWLEDGMENTS

■ REFERENCES

(1) (a) Mishra, A.; Bäuerle, P. *Angew. Chem., Int. Ed.* **2012**, *51*, 2020. (b) Walker, B.; Kim, C.; Nguyen, T.-Q. *Chem. Mater.* **2011**, *23*, 470. (c) Zhang, F.; Wu, D.; Xu, Y.; Feng, X. *J. Mater. Chem.* **2011**, *21*, 17590. (d) Li, Y.; Guo, Q.; Li, Z.; Pei, J.; Tian, W. *Energy Environ. Sci.* **2010**, *3*, 1427. (e) Kanibolotsky, A. L.; Perepichka, I. F.; Skabara, P. J. *Chem. Soc. Rev.* **2010**, *39*, 2695. (f) Zhang, F.; Wu, D.; Xu, Y.; Feng, X. *J. Mater. Chem.* **2011**, *21*, 17590.

(2) (a) Dennler, G.; Scharber, M. C.; Ameri, T.; Denk, P.; Forberich, K.; Waldauf, C.; Brabec, C. J. *Adv. Mater.* **2008**, *20*, 579. (b) Yong, X.; Zhang, J. *J. Mater. Chem.* **2011**, *21*, 11159. (c) Thompson, B. C.; Fréchet, J. M. *Angew. Chem., Int. Ed.* **2008**, *47*, 58.

(3) (a) Moulé, A. J.; Meerholz, K. *Adv. Funct. Mater.* **2009**, *19*, 3028. (b) Peet, J.; Senatore, M. L.; Heeger, A. J.; Bazan, G. C. *Adv. Mater.* **2009**, *21*, 1521. (c) Beaujuge, P. M.; Fréchet, J. M. *J. Am. Chem. Soc.* **2011**, *133*, 20009.

(4) (a) Fitzner, R.; Mena-Osteritz, E.; Mishra, A.; Schulz, G.; Reinold, E.; Weil, M.; Korner, C.; Ziehlke, H.; Elschner, C.; Leo, K.; Riede, M.; Pfeiffer, M.; Uhrich, C.; Bauerle, P. *J. Am. Chem. Soc.* **2012**, *134*, 11064. (b) Lin, L. Y.; Chen, Y. H.; Huang, Z. Y.; Lin, H. W.;

Chou, S. H.; Lin, F.; Chen, C. W.; Liu, Y. H.; Wong, K. T. *J. Am. Chem. Soc.* **2011**, *133*, 15822.

(5) (a) Rivnay, J.; Mannsfeld, S. C.; Miller, C. E.; Salleo, A.; Toney, M. F. *Chem. Rev.* **2012**, *112*, 5488. (b) Cho, E.; Risko, C.; Kim, D.; Gysel, R.; Miller, N. C.; Breiby, D. W.; McGehee, M. D.; Toney, M. F.; Kline, R. J.; Bredas, J. L. *J. Am. Chem. Soc.* **2012**, *134*, 6177. (c) Collins, B. A.; Cochran, J. E.; Yan, H.; Gann, E.; Hub, C.; Fink, R.; Wang, C.; Schuettfort, T.; McNeill, C. R.; Chabinyc, M. L.; Ade, H. *Nat. Mater.* **2012**, *11*, 536. (d) Jinnai, H.; Spontak, R. J. *Polymer* **2009**, *50*, 1067.

(6) (a) Zade, S. S.; Zamoshchik, N.; Bendikov, M. *Acc. Chem. Res.* **2011**, *44*, 14. (b) Henson, Z. B.; Müllen, K.; Bazan, G. C. *Nat. Chem.* **2012**, *4*, 699. (c) Kim, C.; Liu, J.; Lin, J.; Tamayo, A. B.; Walker, B.; Wu, G.; Nguyen, T.-Q. *Chem. Mater.* **2012**, *24*, 1699.

(7) (a) Cheng, Y.-J.; Yang, S.-H.; Hsu, C.-S. *Chem. Rev.* **2009**, *109*, 5868. (b) Carsten, B.; He, F.; Son, H. J.; Xu, T.; Yu, L. *Chem. Rev.* **2011**, *111*, 1493. (c) Chen, J.; Cao, Y. *Acc. Chem. Res.* **2009**, *42*, 1709. (d) Bilby, D.; Kim, B. G.; Kim, J. *Pure Appl. Chem.* **2011**, *83*, 127. (e) Gendron, D.; Leclerc, M. *Energ. Environ. Sci.* **2011**, *4*, 1225.

(8) (a) Liu, X.; Wen, W.; Bazan, G. C. *Adv. Mater.* **2012**, *24*, 4505. (b) Seo, J. H.; Gutacker, A.; Sun, Y.; Wu, H.; Huang, F.; Cao, Y.; Scherf, U.; Heeger, A. J.; Bazan, G. C. *J. Am. Chem. Soc.* **2011**, *133*, 8416. (c) Park, H.-Y.; Yang, H.; Choi, S.-K.; Jang, S.-Y. *ACS Appl. Mater. Interfaces* **2012**, *4*, 214. (d) Li, H.; Tang, H.; Li, L.; Xu, W.; Zhao, X.; Yang, X. *J. Mater. Chem.* **2011**, *21*, 6563. (e) Graham, K. R.; Mei, J.; Stalder, R.; Shim, J. W.; Cheun, H.; Steffy, F.; So, F.; Kippelen, B.; Reynolds, J. R. *ACS Appl. Mater. Interfaces* **2011**, *3*, 1210.

(9) (a) Carroll, G. T.; Sojka, M. E.; Lei, X.; Turro, N. J.; Koberstein, J. T. *Langmuir* **2006**, *22*, 7748.

(10) (a) Sun, Y.; Welch, G. C.; Leong, W. L.; Takacs, C. J.; Bazan, G. C. *Nat. Mater.* **2012**, *11*, 44. (b) van der Poll, T. S.; Love, J. A.; Nguyen, T.-Q.; Bazan, G. C. *Adv. Mater.* **2012**, *24*, 3646. (c) Zhou, J.; Wan, X.; Liu, Y.; Zuo, Y.; Li, Z.; He, G.; Long, G.; Ni, W.; Li, C.; Su, X.; Chen, Y. *J. Am. Chem. Soc.* **2012**, *134*, 16345. (d) Takacs, C. J.; Sun, Y.; Welch, G. C.; Perez, L. A.; Liu, X.; Wen, W.; Bazan, G. C.; Heeger, A. J. *J. Am. Chem. Soc.* **2012**, *134*, 16597.

(11) Zhou, H.; Yang, L.; Price, S. C.; Knight, K. J.; You, W. *Angew. Chem., Int. Ed.* **2010**, *49*, 7992.

(12) (a) Bashir, Z.; Khan, N.; Price, D. M. *Thermochim. Acta* **1998**, *319*, 47. (b) Perez, E.; Rinde, E.; Bello, A.; Benavente, R.; Perena, J. M. *Macromolecules* **1992**, *25*, 605.

(13) (a) Russell, T. P. *Mater. Sci. Rep.* **1990**, *5*, 171. (b) Chasona, E.; Mayera, T. M. *Crit. Rev. Solid State* **1997**, *22*, 1. (c) Huang, T. C.; Gilles, R.; Will, G. *Thin Solid Films* **1993**, *230*, 99.

(14) (a) Meyer, J.; Khalandovsky, R.; Görrn, P.; Kahn, A. *Adv. Mater.* **2011**, *23*, 70. (b) Sun, Y.; Takacs, C. J.; Cowan, S. R.; Seo, J. H.; Gong, X.; Roy, A.; Heeger, A. J. *Adv. Mater.* **2011**, *23*, 2226. (c) Girotto, C.; Voroshazi, E.; Cheyns, D.; Heremans, P.; Rand, B. P. *ACS Appl. Mater. Interfaces* **2011**, *3*, 3244. (d) Murase, S.; Yang, Y. *Adv. Mater.* **2012**, *24*, 2459. (e) Shrotriya, V.; Li, G.; Yao, Y.; Chu, C.-W.; Yang, Y. *Appl. Phys. Lett.* **2006**, *88*, 073508.

(15) Zhou, J.; Wan, X.; Liu, Y.; Long, G.; Wang, F.; Li, Z.; Zuo, Y.; Li, C.; Chen, Y. *Chem. Mater.* **2011**, *23*, 4666.

(16) (a) Welch, G. C.; Perez, L. A.; Hoven, C. V.; Zhang, Y.; Dang, X.-D.; Sharenko, A.; Toney, M. F.; Kramer, E. J.; Nguyen, T.-Q.; Bazan, G. C. *J. Mater. Chem.* **2011**, *21*, 12700. (b) Liu, Y.; Wan, X.; Wang, F.; Zhou, J.; Long, G.; Tian, J.; Chen, Y. *Adv. Mater.* **2011**, *23*, 5387. (c) Loser, S.; Bruns, C. J.; Miyauchi, H.; Ortiz, R. P.; Facchetti, A.; Stupp, S. I.; Marks, T. J. *J. Am. Chem. Soc.* **2011**, *133*, 8142. (d) Lee, O. P.; Yiu, A. T.; Beaujuge, P. M.; Woo, C. H.; Holcombe, T. W.; Millstone, J. E.; Douglas, J. D.; Chen, M. S.; Fréchet, J. M. J. *Adv. Mater.* **2011**, *23*, 5359.

(17) (a) Li, W.; Roelofs, W. S.; Wienk, M. M.; Janssen, R. A. *J. Am. Chem. Soc.* **2012**, *134*, 13787. (b) Zhou, H.; Yang, L.; Stuart, A. C.; Price, S. C.; Liu, S.; You, W. *Angew. Chem., Int. Ed.* **2011**, *50*, 2995. (c) Wang, M.; Hu, X.; Liu, P.; Li, W.; Gong, X.; Huang, F.; Cao, Y. *J. Am. Chem. Soc.* **2011**, *133*, 9638. (d) Wang, E.; Ma, Z.; Zhang, Z.; Vandewal, K.; Henriksson, P.; Inganäs, O.; Zhang, F.; Andersson, M. R. *J. Am. Chem. Soc.* **2011**, *133*, 14244. (e) Peng, Q.; Liu, X.; Su, D.; Fu, G.; Xu, J.; Dai, L. *Adv. Mater.* **2011**, *23*, 4554.